Behavioral/Systems/Cognitive

The Persistent Sodium Current Generates Pacemaker Activities in the Central Pattern Generator for Locomotion and Regulates the Locomotor Rhythm

Sabrina Tazerart, Laurent Vinay, and Frédéric Brocard

Laboratoire Plasticité et Physio-Pathologie de la Motricité, Unité Mixte de Recherche 6196, Centre National de la Recherche Scientifique, Université Aix-Marseille, F-13402 Marseille Cedex 20, France

Rhythm generation in neuronal networks relies on synaptic interactions and pacemaker properties. Little is known about the contribution of the latter mechanisms to the integrated network activity underlying locomotion in mammals. We tested the hypothesis that the persistent sodium current (I_{NaP}) is critical in generating locomotion in neonatal rodents using both slice and isolated spinal cord preparations. After removing extracellular calcium, 75% of interneurons in the area of the central pattern generator (CPG) for locomotion exhibited bursting properties and I_{NaP} was concomitantly upregulated. Putative CPG interneurons such as commissural and Hb9 interneurons also expressed I_{NaP}-dependent (riluzole-sensitive) bursting properties. Most bursting cells exhibited a pacemaker-like behavior (i.e., burst frequency increased with depolarizing currents). Veratridine upregulated I_{NaP}, induced riluzole-sensitive bursting properties, and slowed down the locomotor rhythm. This study provides evidence that I_{NaP} generates pacemaker activities in CPG interneurons and contributes to the regulation of the locomotor activity.

Key words: **neonatal rat; spinal cord; locomotion; central pattern generator; rhythm; riluzole**

Introduction

In vertebrates, the locomotor activity in hindlimb muscles is generated by central pattern generator (CPG) networks located within the spinal cord. CPGs must fulfill two tasks: they generate the rhythm ("clock") and produce the appropriate sequences of muscle activation ("pattern") with alternating contractions of flexor and extensor muscles and alternation between left and right hindlimb movements. In most networks, rhythm and pattern generations rely on two types of mechanisms: the emergent-network and the pacemaker-neuronal mechanisms (Arshavsky, 2003; Ramirez et al., 2004; Grillner, 2006). Our knowledge of the contribution of pacemaker properties (and the underlying ionic currents) to locomotor rhythm generation in mammals is still very fragmentary. There is increasing evidence that the primary neuronal kernel for locomotor rhythm generation is restricted to the ventromedial gray matter of upper lumbar segments in rodents (Cazalets et al., 1995; Kjaerulff and Kiehn, 1996). This spinal region contains conditional pacemaker cells characterized by intrinsic bursting properties that are induced by activating NMDA receptors and independent of sodium currents (Hochman et al., 1994; Kiehn et al., 1996; Wilson et al., 2005). Although hypothesized to be involved in rhythmogenesis (Schmidt et al., 1998), these sodium-independent bursting properties are not sufficient by themselves to generate the locomotor rhythm because a specific blockade of the persistent sodium current (I_{NaP}) abolishes fictive locomotion (Tazerart et al., 2007b; Zhong et al., 2007) and furthermore mostly depresses the disinhibited locomotor-like rhythm (Darbon et al., 2004; Taccola and Nistri, 2007). I_{NaP} is ubiquitously associated with pacemaker properties in a variety of supraspinal neuronal populations (Thoby-Brisson and Ramirez, 2001; Del Negro et al., 2005; Brocard et al., 2006; van Drongelen et al., 2006). If pacemaker neurons are assumed to be important in the operation of mammalian locomotor CPG (Rybak et al., 2006; McCrea and Rybak, 2007), then I_{NaP}-dependent bursting properties should exist in the spinal cord. The widespread expression of the I_{NaP} in the locomotor CPG region (Tazerart et al., 2007b; Theiss et al., 2007), and particularly in commissural interneurons (Zhong et al., 2007) critical for left–right coordination of locomotor movements (Butt and Kiehn, 2003), supports this hypothesis.

The present study was aimed at investigating whether a modulation of I_{NaP} promotes a pacemaker activity in interneurons considered to be part of the locomotor CPG (commissural and Hb9 interneurons), and determining its contribution to the operation of the locomotor circuitry. We report that upregulating I_{NaP} makes most interneurons switch from a regular-spiking pattern into a pacemaker-like bursting mode and slows down the fictive locomotor rhythm. We thus provide the first description of pacemaker properties independent of both Ca^{2+} channels and NMDA receptors in the mammalian locomotor CPG. We dem-

Received April 4, 2008; revised June 4, 2008; accepted July 2, 2008.

This work was supported by the French National Research Agency ("Neurosciences, Neurologie et Psychiatrie" Program) and the French Institut pour la Recherche sur la Moelle Epinière et l'Encéphale (S.T.). We are grateful to Sylvie Liabeuf, Cécile Brocard, and Marie Gardette for their technical assistance.

Correspondence should be addressed to Dr. Frédéric Brocard, Laboratoire Plasticité et Physio-Pathologie de la Motricité, Unité Mixte de Recherche 6196, Centre National de la Recherche Scientifique, 31 chemin Joseph Aiguier, F-13402 Marseille Cedex 20, France. E-mail: brocard@dpm.cnrs-mrs.fr.

DOI:10.1523/JNEUROSCI.1437-08.2008

 0270-6474/08/288577-13$15.00/0

onstrate that I_{NaP} plays a significant role in generating the locomotor rhythm: the regulation of I_{NaP}-dependent pacemaker activity may provide a mechanism by which the locomotor rhythm is finely tuned. Preliminary report of these findings has been published in abstract form (Tazerart et al., 2007a).

Materials and Methods

Experiments were performed on neonatal (1–5 d of age) Wistar rats ($n = 84$) and Hb9:eGFP transgenic mice ($n = 5$) (Wichterle et al., 2002). All surgical and experimental procedures conformed to guidelines from the French Ministry for Agriculture and Fisheries.

In vitro *preparations.* Rodents were anesthetized by hypothermia and decapitated. For the whole spinal cord preparation, the spinal cord was isolated as described in detail previously (Brocard et al., 1999), transected at T10, and transferred to the recording chamber, which was perfused with oxygenated normal Krebs' solution composed of the following (in mM): 130 NaCl, 4 KCl, 3.75 $CaCl_2$, 1.3 $MgSO_4$, 0.58 NaH_2PO_4, 25 $NaHCO_3$, 10 glucose, pH 7.4 (24–26°C). A Vaseline barrier was built at the L2/L3 level to superfuse the most important part of the locomotor CPG (Cazalets et al., 1995; Hsiao et al., 1998; Kiehn, 2006) independently from the motoneurons recorded at the L5 level. For the slice preparation, the lumbar spinal cord was isolated in oxygenated (95% O_2/5% CO_2) ice-cold (<4°C) artificial CSF (ACSF) solution composed of the following (in mM): 232 sucrose, 3 KCl, 1.25 KH_2PO_4, 4 $MgSO_4$, 0.2 $CaCl_2$, 26 $NaHCO_3$, 25 D-glucose, pH 7.4. The lumbar spinal cord was then introduced into a 1% agar solution and quickly cooled. Transverse slices (350 μm) through the L1–L2 lumbar segments were obtained and transferred into the holding chamber filled with oxygenated ACSF consisting of the following (in mM): 120 NaCl, 3 KCl, 1.25 NaH_2PO_4, 1.3 $MgSO_4$, 1.2 $CaCl_2$, 25 $NaHCO_3$, 40 D-glucose, pH 7.4 (24–26°C). Slices were allowed to equilibrate for ~1 h and transferred to an immersion slice chamber, perfused with the oxygenated solution thermoregulated at 25°C (2 ml/min). To label descending commissural interneurons in transverse slices (see Fig. 5*A1*), slits were made in the caudal contralateral hemicord (L3–L4) of the intact preparation, and crystals of 3000 molecular weight fluorescein dextran amine were placed in the slits. After incubation for 1–2 h to allow the retrogradely transport of the dyes to the somata, slices were prepared as described above.

Recordings. Electrophysiological data were acquired through a Digidata 1322A interface using the Clampex 9 software (Molecular Devices). For the whole spinal cord preparation, the locomotor-like activity was recorded (bandwidth, 70 Hz to 1 kHz) using extracellular stainless-steel electrodes placed in contact with lumbar ventral roots (left/right L5) and insulated with Vaseline. For the slice preparation, neurons were visualized using differential interference contrast optics of a fixed-stage microscope (Eclipse E600FN; Nikon) coupled with a 40× water-immersion lens. The image was enhanced with an infrared-sensitive CCD camera and displayed on a video monitor. To assure the accuracy of the neuron location, the ventral one-half of the spinal cord was divided in quadrants as defined by previous authors (Theiss and Heckman, 2005). All interneurons were recorded in the dorsomedial quadrant. Thus, most of the interneurons were recorded in laminas VII–VIII. In this restricted area, fluorescein-labeled neurons contralateral to the dye injection site (see above) were visualized under epifluorescent illumination and identified as descending commissural interneurons. In transgenic Hb9:eGFP transgenic mice, small clustered GFP-positive interneurons located in the medial lamina VIII and adjacent to the central canal were selected in our recordings to avoid Hb9-negative interneurons (Wilson et al., 2007). Only GFP-positive interneurons compatible with the previously described electrophysiological profile of Hb9 interneurons (i.e., high input resistance, strong postinhibitory rebound, and absence of sag) were considered (Wilson et al., 2005). Whole-cell patch-clamp recordings in current- and voltage-clamp mode were performed with a Multiclamp 700B amplifier (Molecular Devices). Patch electrodes (4–6 MΩ) were pulled from borosilicate glass capillaries (1.5 mm outer diameter, 1.12 mm inner diameter; World Precision Instruments) on a Sutter P-97 puller (Sutter Instrument) and filled with intracellular solution containing the following (in mM): 140 K^+-gluconate, 5 NaCl, 2 $MgCl_2$, 10 HEPES, 0.5 EGTA, 2 ATP, 0.4 GTP, pH 7.3 (280–290 mOsm). After the establishment of a gigaseal, the pipette resistance and capacitance were compensated electronically. After the membrane was ruptured, the green fluorescent diffusion into the tip of the patch-clamp pipette confirmed that recordings were performed in interneurons considered to be part of the locomotor CPG (see Fig. 5*A2*, inset). As observed in our previous study (Tazerart et al., 2007), injection of a small negative current (−10 to −20 pA) was necessary to prevent most of interneurons to fire spontaneously and hold them at −70 mV. Recordings were digitized on-line and filtered at 10 kHz (current clamp) and at 4 kHz (voltage clamp). The junction potential (~14 mV) was corrected off-line based on the composition of the internal and external solutions used for recordings. To isolate cells from the network inputs, Ca^{2+} was removed from the extracellular solution. Note that Ca^{2+} was substituted by Mg^{2+} to avoid any changes in the osmolarity known to influence bursting properties (Azouz et al., 1997). Interneurons were sometimes isolated from most rapid synaptic inputs with a combination of kynurenic acid (1.5 mM), biccuculine (20 μM), and strychnine (1 μM) to block glutamatergic, fast GABAergic, and glycinergic synapses, respectively. To isolate Na^+ currents during voltage-clamp experiments, we used a modified ACSF containing the following (in mM): 100 NaCl, 3 KCl, 1.25 NaH_2PO_4, 1.3 $MgSO_4$, 3.6 $MgCl_2$, 1.2 $CaCl_2$, 25 $NaHCO_3$, 40 D-glucose, 10 tetraethylammonium-Cl, and 0.1 $CdCl_2$. The main characterization of I_{NaP} was accomplished with triangular voltage-clamp commands from −70 to −10 mV and back, slow enough (12 mV/s) to prevent transient sodium channel opening in most of the recorded interneurons; those in which transient sodium currents occurred were discarded from this study. Action potential-independent miniature EPSCs (mEPSCs) and miniature IPSCs (mIPSCs) were recorded in the presence of tetrodotoxin (TTX) (1 μM) at a holding potential of −70 mV. As previously performed in the neonatal rat slice preparation (Gao et al., 2001), experiments were performed in high extracellular K^+ (20 mM) to acquire sufficient sample of miniature PSCs (mPSCs). NMDA and non-NMDA receptor-mediated mEPSCs were recorded with a K^+-gluconate based intracellular solution (see above) and pharmacologically isolated with a combination of strychnine (1 μM) and biccuculine (20 μM). Glycine and GABA receptor-mediated mIPSCs were recorded with an internal solution composed of the following (in mM): 110 CsCl, 30 KCl, 5 NaCl, 2 $MgCl_2$, 10 HEPES, 0.5 EGTA, 2 ATP, 0.4 GTP, pH 7.3 with CsOH; and pharmacologically isolated in the presence of kynurenic acid (1.5 mM).

Data analysis. Electrophysiological data were analyzed with Clampfit 9 software (Molecular Devices). Only cells exhibiting a stable resting or holding membrane potential and an action potential amplitude >45 mV were considered. Passive membrane properties of cells were measured by determining from the holding potential the largest voltage deflections induced by small currents pulses to avoid the activation of voltage-sensitive currents. The rheobase was defined as the minimum current intensity required to induce action potential during a 1 s pulse. Single spike analysis was performed on the first spike elicited near the rheobase. Peak spike amplitude was measured from the threshold potential, and spike duration was defined as the time to fall to half-maximum peak. We defined the voltage-dependent activation threshold of the I_{NaP} as the membrane potential at which the slope of leak-subtracted current becomes negative. We measured the magnitude of I_{NaP} as the peak of the leak-subtracted inward current during the ascending and the descending phase of the voltage command. mPSCs were detected and analyzed using the MiniAnalysis Program (Synaptosoft). Events were detected by setting the threshold value for detection at three times the level of the root mean square noise (~3–4 pA meaning detection threshold at ~8–12 pA). The average values of mPSCs amplitude and frequency during the control period and 20 min after the drug application, were calculated over a 5 min time window.

Alternating activity between right/left L5 recordings was taken to be indicative of fictive locomotion. During an episode of fictive locomotion, cycle periods shortened progressively and reached a steady state within 5 min (data not shown) (Sqalli-Houssaini et al., 1993; Cazalets et al., 1999). From this time, a 5 min period of locomotor-like activity was analyzed. Raw extracellular recordings from ventral roots were rectified and resampled at 50 Hz. Amplitude and duration of ventral root bursts were

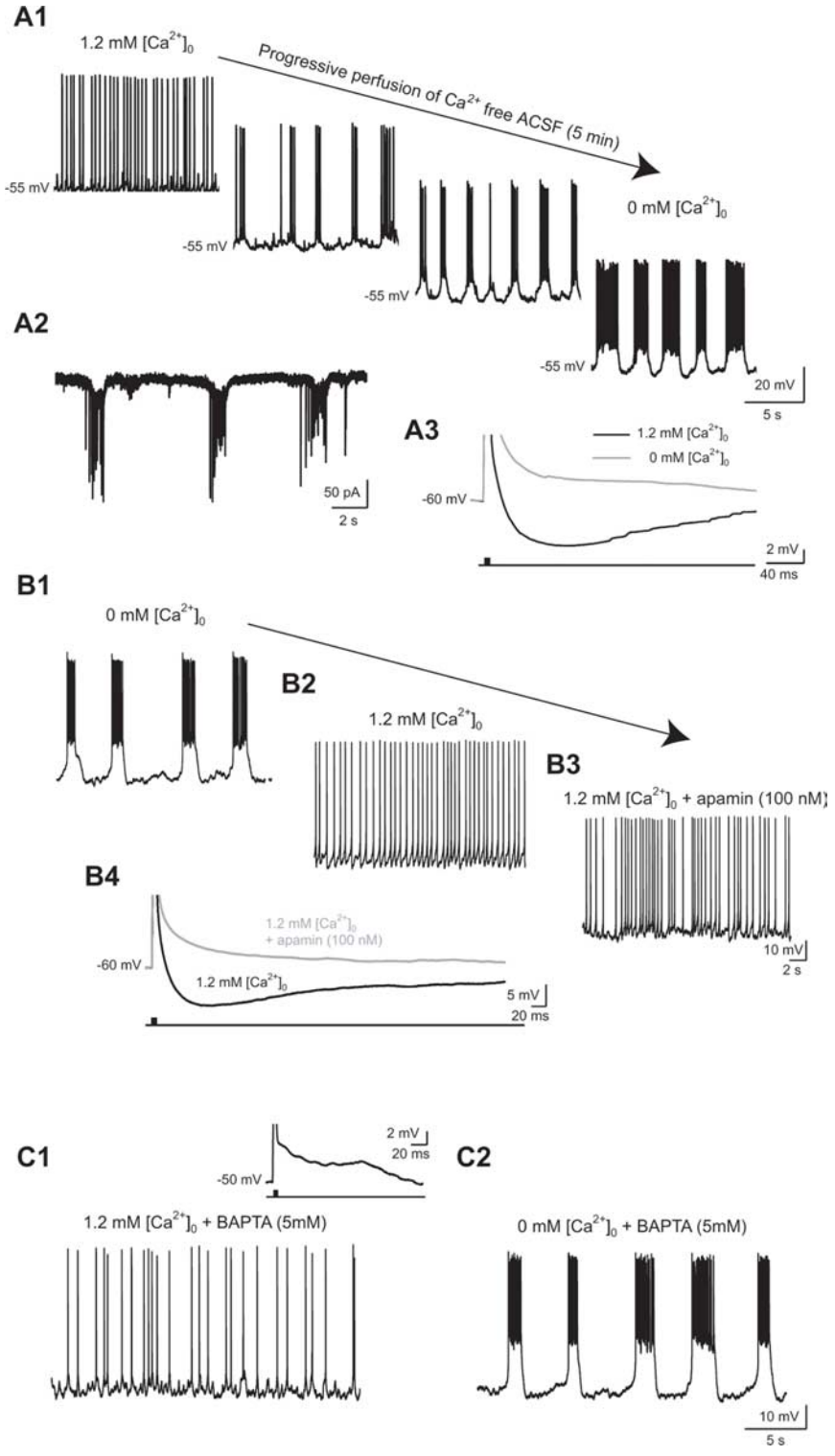

Figure 1. Intrinsic bursting properties that emerge in upper lumbar ventromedial interneurons by removing $[Ca^{2+}]_o$ are related neither to small Ca^{2+}-activated K^+ conductance nor to intracellular Ca^{2+} processes. ***A1***, Voltage traces showing a typical ventromedial interneuron switching its firing pattern from tonic spiking to bursting after a progressive depletion of the $[Ca^{2+}]_o$. ***A2***, Repetitive events recorded in the cell-attached configuration from the surface of a bursting ventromedial interneuron. ***A3***, Slow afterhyperpolarizations after a spike (truncated) evoked by a 3 ms current pulse (bottom trace) before (black trace) and after removing $[Ca^{2+}]_o$ (gray trace). Each trace in ***A3*** represents the average of three sweeps. The initial holding potential was −60 mV. ***B1–B3***, Voltage traces from a ventromedial interneuron exhibiting a bursting behavior in $[Ca^{2+}]_o$-free ACSF (***B1***) but not in 1.2 mM $[Ca^{2+}]_o$ (***B2***) even after bath application of 100 nM apamin (***B3***). ***B4***, Voltage traces (average of 3 sweeps) showing slow afterhyperpolarizations that follow spikes (truncated) evoked by a 3 ms current pulse (bottom trace) before (black trace) and after 100 nM apamin (gray trace). The initial holding potential was −60 mV. ***C1***, ***C2***, Voltage traces of a neuron recorded by means of an electrode filled with BAPTA (5 mM) before (***C1***) and after the removal of the extracellular calcium (***C2***). The inset (3 sweeps averaged) in ***C1*** shows the absence of slow afterhyperpolarizations after spikes (truncated) evoked by a 3 ms current pulse. The initial holding potential was −50 mV.

measured by a threshold function that determines the peak, the onset, and end of bursts of activity. The threshold was usually set to ~30% of the peak value. The cycle period was calculated by measuring the distance between the first two peaks of the autocorrelogram. Cross-correlation analysis was performed to measure the coupling between the left and right L5 ventral bursts during the different experimental conditions. The quality of the alternation was estimated by measuring the negative correlation coefficient at zero phase lag (center of the cross-correlogram). Details about the autocorrelation and cross-correlation analysis have been described previously (Madriaga et al., 2004; Pearlstein et al., 2005).

Data are presented as means ± SEM. Effects (e.g., on peak current) are sometimes expressed as a percentage of the control currents. Nonparametric statistical analysis were used with a Mann–Whitney test or a Wilcoxon matched-pair test when two groups were compared and a one-way ANOVA followed by a Tukey test for multiple-group comparisons. The statistical test used is mentioned in the text. Values of $p < 0.05$ were considered significant (GraphPad Software).

Drug application. The following pharmacological agents from Sigma-Aldrich were used: riluzole (10 μM), veratridine (20–500 nM), carbenoxolone (200 μM), strychnine (1 μM), bicuculline (20 μM), acid kynurenic (1.5 mM), *N*-methyl-DL-aspartic acid (NMA) (15 μM), 5-hydroxytryptamine creatinine sulfate (5-HT) (5 μM), TTX (0.5–1 μM), apamin (100 nM), BAPTA-AM (50 μM), BAPTA (5 mM), and 4-(*N*-ethyl-*N*-phenylamino)-1,2-dimethyl-6-(methylamino)pyridinium chloride (ZD 7288) (20 μM). Riluzole was dissolved in dimethylsulfoxide (DMSO) and added to the ACSF (final concentration of DMSO, 0.1%). Vehicle control experiments showed no differences on bursting properties (data not shown).

Results

Intrinsic bursting properties emerge in the absence of extracellular calcium ($[Ca^{2+}]_o$)

The initial set of experiments was performed to assess whether interneurons located in the locomotor CPG region exhibit I_{NaP}-dependent bursting properties. Whole-cell patch-clamp recordings were performed from unidentified interneurons located in the ventromedial gray matter of upper (L1–L2) lumbar segments. To isolate cells from the rest of the circuitry, we removed calcium from extracellular solution. This protocol enables to both abolish synaptic transmission and prevent bursting properties that rely on Ca^{2+}-dependent mechanisms. As demonstrated in our previous study (Tazerart et al. 2007b), none of the interneurons recorded with 1.2 mM $[Ca^{2+}]_o$ displayed bursting properties. The most obvious effect of removing Ca^{2+} was that 75% of cells (45 of

59) acquired bursting properties in response to current injection close to rheobase (Fig. 1*A1*), whereas the remaining nonbursting cells exhibited a tonic spiking activity (data not shown). The persistence of bursting activity after the blockade of fast synaptic transmission by kynurenic acid (1.5 mM), bicuculline (20 μM), and strychnine (1 μM), precluded a role of synaptic inputs in the generation of bursts (Fig. 2*B2*). Intrinsic bursting properties were not attributable to intracellular dialyzation bias because bursts were also observed in the cell-attached configuration (Fig. 1*A2*). The acquisition of bursting properties occurred without any significant alteration in input resistance (1023 ± 323 vs 977 ± 185 MΩ; Wilcoxon's paired test, $p > 0.05$; $n = 11$) but with a concomitant abolition of slow afterhyperpolarizations (AHPs) (Fig. 1*A3*), a major feature of ventromedial interneurons (Tazerart et al., 2007b). In the presence of 1.2 mM $[Ca^{2+}]_o$, the complete blockade of slow AHPs with 100 nM apamin (Fig. 1*B4*), a selective blocker of the small conductance Ca^{2+}-activated K^+ channels, did not convert tonic spiking activity (Fig. 1*B2*) to bursting (Fig. 1*B3*). The latter effect did not result from the inability of the cells to burst because the same neuron generated bursts in $[Ca^{2+}]_o$-free ACSF (Fig. 1*B1*). As an additional test for the absence of contribution of Ca^{2+}-activated currents to the generation of bursts, chelation of intracellular Ca^{2+} was performed with 5 mM BAPTA intrapipette. In this condition, none of the neurons ($n = 8$) recorded in 1.2 mM $[Ca^{2+}]_o$ displayed slow AHPs (Fig. 1*C1*, inset), suggesting an effective chelation of intracellular Ca^{2+} by BAPTA. Intracellular diffusion of BAPTA did not generate bursts (Fig. 1*C1*). When the extracellular calcium was removed, BAPTA did not prevent the emergence of bursts that persisted as long as the cell was recorded (at least 30 min) (Fig. 1*C2*). Similar results were also obtained in six neurons after BAPTA-AM had been preincubated for >1 h (data not shown). Together, these results suggest that cellular mechanisms underlying bursting properties are independent of both voltage-sensitive Ca^{2+} channels and the release of Ca^{2+} from intracellular stores.

The major property that characterized bursting neurons was their higher excitability, as shown by a lower firing threshold ($p < 0.05$, Mann–Whitney's test) (Table 1) (note also the nonsignificant trend toward a lower rheobase). In agreement with such observations, I_{NaP} has been shown to play a significant role in the

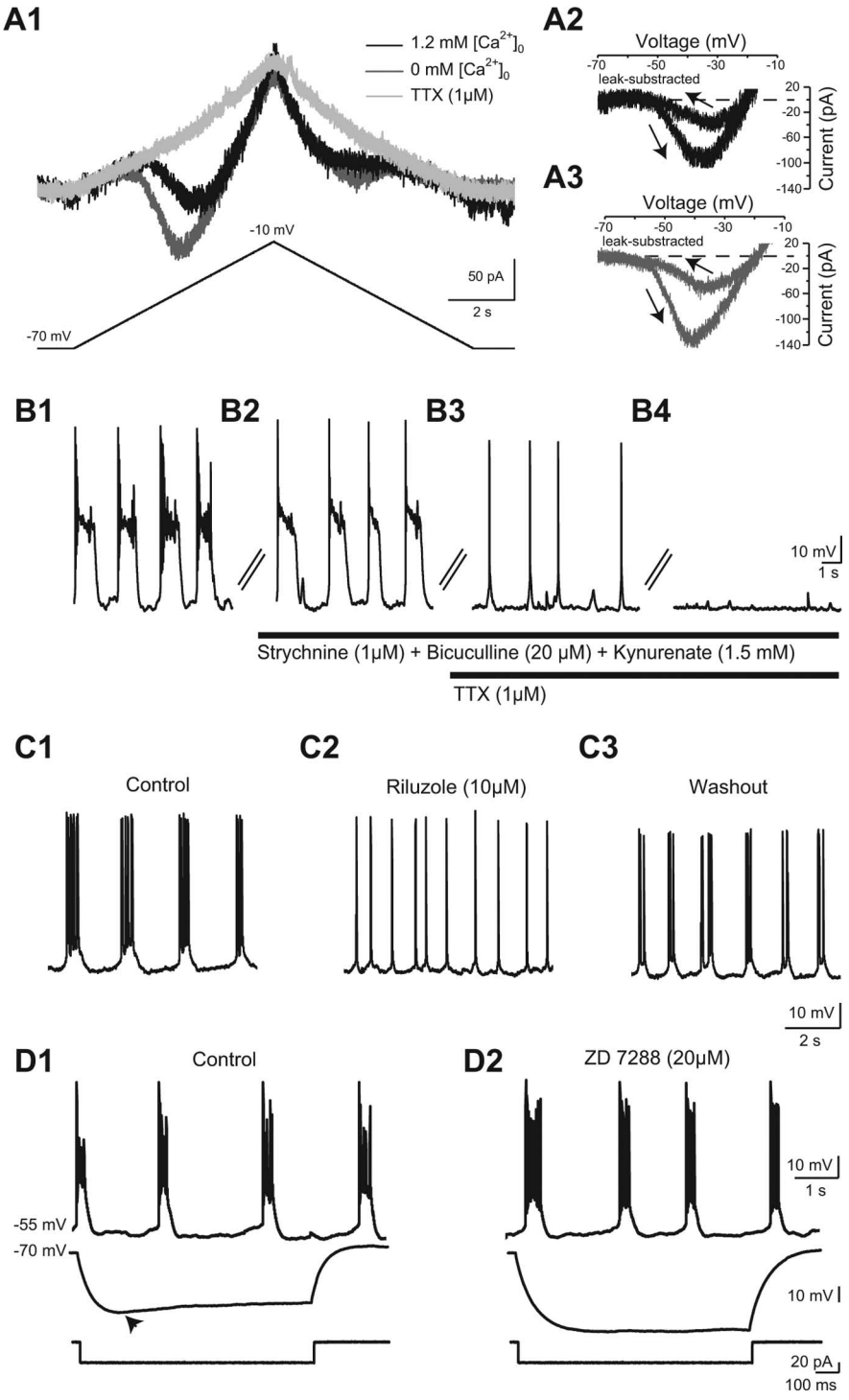

Figure 2. Dependence of bursting properties on I_{NaP} but not on I_h. ***A1***, Total membrane current (top traces) evoked by a triangular voltage ramps (bottom trace) from −70 to +10 mV and back to −70 mV over 10 s, before (black trace) and after removing the extracellular calcium (dark gray trace). A subsequent application of TTX (1 μM) abolished the current (light gray trace). ***A2***, ***A3***, The current leak-subtracted was plotted as a function of command voltage in the presence (***A2***) and absence of extracellular calcium (***A3***). The arrows indicate direction of voltage changes. ***B1***, ***B2***, Effects of sodium currents blockade on bursting properties. A ventromedial interneuron displaying bursting properties in $[Ca^{2+}]_o$-free ACSF is illustrated before (***B1***) and 20 min (***B2***) after the application of strychnine (1 μM), bicuculline (20 μM), and kynurenate (1.5 mM). ***B3*** and ***B4*** illustrate the effect of a progressive blockade of sodium currents on the burst generation, 5 and 10 min after the onset of TTX application (1 μM), respectively. ***C1***, ***C2***, Effects of a blockade of I_{NaP} on bursting properties. Another ventromedial interneuron exhibiting bursting properties in $[Ca^{2+}]_o$-free ACSF is illustrated before (***C1***) and 15 min (***C2***) after the application of riluzole (10 μM). Note in ***C2*** that the amplitude of spikes was not affected. In ***C3***, a recovery of bursting properties is illustrated after a 1 h washout period. ***D1***, ***D2***, Effects of a blockade of I_h on bursting properties. A ventromedial interneuron exhibiting bursting properties in $[Ca^{2+}]_o$-free ACSF is illustrated before (***D1***) and 15 min (***D2***) after the application of ZD 7288 (20 μM). ZD 7288 blocked the depolarizing sag (arrowhead) induced by a hyperpolarizing current pulse of −0.4 nA.

Table 1. Membrane properties of ventromedial interneurons classified on the basis of their firing patterns

	Bursters	Nonbursters
n	45	14
R_m (MΩ)	844 ± 91	705 ± 108
AP amp (mV)	57.6 ± 1.5	62.5 ± 2.8
AP dur (ms)	2.3 ± 0.1	1.9 ± 0.15
AP threshold (mV)	−45.2 ± 1.0	−41.6 ± 1.2*
Rheobase (pA)	17.8 ± 3.2	22.6 ± 5.8

n represents the number of cells. AP, Action potential; amp, amplitude; dur, duration.

*$p < 0.05$. Statistical significance was assessed by a Mann–Whitney test.

modulation of neuronal excitability by setting the threshold of firing (Crill, 1996). Because I_{NaP} is the main slow inward currents in ventromedial interneurons (Tazerart et al., 2007b; Theiss et al., 2007; Zhong et al., 2007), we investigated further the role of this current in the emergence of bursting.

Bursting properties emerge with a concomitant increase of I_{NaP}

The relationship between biophysical properties of I_{NaP} and $[Ca^{2+}]_o$ was examined by means of voltage-clamp recordings. Recordings were made under conditions designed to minimize voltage-gated calcium and potassium currents to isolate I_{NaP} (see Materials and Methods). In response to slow triangular voltage ramp commands, the 12 ventromedial neurons tested typically displayed a large inward voltage-dependent current (Fig. 2*A1*, black trace). This inward current was likely attributable to I_{NaP} because it was abolished by riluzole (10 μM) or TTX (1 μM) (Fig. 2*A1*, pale gray trace). On the ascending *I–V* function (Fig. 2*A2*), the mean voltage-dependent activation threshold of I_{NaP} was −55.8 ± 1.7 mV and I_{NaP} peaked in amplitude at 45 ± 9 pA. On the descending *I–V* function (Fig. 2*A2*), I_{NaP} peaked in amplitude at 27 ± 9 pA. The progressive depletion of $[Ca^{2+}]_o$ induced a consistent leftward shift of the *I–V* relationship (Fig. 2*A1*,*A3*, dark gray trace). Consequently, the voltage activation threshold of I_{NaP} was significantly shifted to more hyperpolarized potentials (−60 ± 1.6 mV; Wilcoxon's paired test, $p < 0.01$). Magnitude of the I_{NaP} on both the ascending and descending phases were also significantly increased by 30 ± 27% (58 ± 12 pA; Wilcoxon's paired test, $p < 0.05$) and 19 ± 38% (32 ± 10 pA; Wilcoxon's paired test, $p < 0.05$), respectively. Raising $[Ca^{2+}]_o$ shifted the voltage dependence of I_{NaP} activation back to more positive potentials (data not shown). As a consequence, in the absence of $[Ca^{2+}]_o$, there is a significant amount of active I_{NaP} within the voltage range from about −60 to −35 mV, whereas in 1.2 mM $[Ca^{2+}]_o$ the activation curve is much more depolarized.

Intrinsic bursting properties depend on I_{NaP}

Shifting the activation curve of I_{NaP} to more negative potentials has been reported to increase bursting abilities of cells (Alkadhi and Tian, 1996; Li and Hatton, 1996; Su et al., 2001). We then examined the role of sodium influx in burst generation. In all the examined bursting neurons ($n = 7$) (Fig. 2*B*), the progressive application of TTX (1 μM) mostly decreased the duration of bursts, whereas single action potentials persisted for few minutes (Fig. 2*B3*). On a longer timescale, all neurons became inactive (Fig. 2*B4*). The delay in the blocking effect of TTX between bursts and spikes may reflect an involvement of I_{NaP} in burst generation. We tested this hypothesis in 19 neurons by applying riluzole at a concentration that specifically blocks I_{NaP} (Tazerart et al., 2007b). Adding 10 μM riluzole to the ACSF abolished the generation of repetitive bursts and converted rhythmic bursting to regular firing without blocking spikes (Fig. 2, compare *C1*, *C2*). This effect reversed after ~1 h of washout (Fig. 2*C3*). The cationic current activated by hyperpolarization, I_h, has been shown to support rhythmogenesis in many models (Pape, 1996). The evidence that the activation curve of I_{NaP} shifts to more negative potentials led us to assess the role that I_h might play in the emergence of bursting activity. ZD 7288 applied at a concentration (20 μM) that blocks the sag did not prevent bursting in Ca^{2+}-free ACSF (Fig. 2*D1*,*D2*) ($n = 5$ of 5). Together, these data strongly demonstrate that bursting in $[Ca^{2+}]_o$-free ACSF is driven predominantly by an upregulation of I_{NaP}, whereas I_h is not critical for burst generation in these conditions.

Discrimination between pacemaker and nonpacemaker cells

Forty-five bursting cells were classified on the basis of their firing patterns in response to depolarizing currents (Fig. 3). The vast majority of them (80%) exhibited a pacemaker-like behavior, the number of bursts increasing with the magnitude of injected currents (Fig. 3*A1*,*A2*, compare middle and top traces; *B1*,*B2*). The mean burst frequency ranged from 0.15 ± 0.02 Hz at near-threshold depolarizations to 0.62 ± 0.07 Hz in response to larger currents. With additional depolarization, the bursting pattern became erratic and switched to a spiking pattern (data not shown). The remaining bursting cells (20%) were considered as nonpacemaker cells (Fig. 3*A3*) because the burst frequency (mean, 0.2 ± 0.1 Hz) was insensitive to the amount of injected current (Fig. 3*A3*, compare middle and top traces; *B3*). Nonpacemaker cells did not differ significantly from pacemaker cells on the basis of basic membrane properties ($p < 0.05$, Mann–Whitney test) (Table 2) (note, however, a trend toward lower input resistance in nonpacemakers cells). At subthreshold potentials, all nonpacemaker cells as well as 40% of pacemaker neurons displayed voltage-insensitive membrane oscillations (Fig. 3*A2*; *A3*, bottom trace). Because they were consistently related to a recurring inward current when the cell was voltage clamped (Fig. 3*C2*,*C3*), these subthreshold membrane oscillations were likely independent of voltage-gated channels in the cell recorded. They might have reflected external driving inputs from gap junction-coupled cells as synaptic transmission was abolished in $[Ca^{2+}]_o$-free ACSF. This hypothesis was confirmed by the application of the gap junction blocker carbenoxolone (200 μM), which abolished both subthreshold membrane oscillations and associated recurring inward currents (Fig. 4*A*, two bottom traces). Furthermore, carbenoxolone disrupted the generation of bursts in nonpacemaker cells (Fig. 4*A*, top trace) but not in pacemaker neurons (Fig. 4*B*).

Putative locomotor CPG interneurons express an I_{NaP}-dependent pacemaker-like behavior

Experiments were conducted to investigate whether an upregulation of I_{NaP} promotes a pacemaker activity in interneurons considered to be part of the locomotor CPG. By their axon projecting contralaterally, commissural interneurons (CINs) are critical for left–right coordination of hindlimb movements (Butt and Kiehn, 2003). They have recently been shown to express I_{NaP} (Zhong et al., 2007) and were thus herein tested for their pacemaker ability. About one-half (five of nine) of dextran-labeled commissural interneurons (Fig. 5*A1*) recorded in $[Ca^{2+}]_o$-free ACSF generated bursts (Fig. 5*B1*), which were sensitive to riluzole (10 μM) (Fig. 5*C1*). Most bursting CINs (four of five) displayed pacemaker-like properties (Fig. 5*B1*) with a relatively wide range of burst frequencies from 0.23 ± 0.11 to 1.17 ± 0.32 Hz. Among

pacemakers, two were silent at hyperpolarized potentials, whereas the others exhibited subthreshold membrane oscillations blocked by carbenoxolone (data not shown). The remaining bursting CIN was a nonpacemaker cell.

Ipsilaterally projecting excitatory interneurons have been hypothesized to be the source of rhythm generation in the locomotor CPG (Kiehn, 2006). A specific class of excitatory locomotor-related interneurons, which express green fluorescent protein under the control of the homeodomain protein HB9 in a transgenic mouse (Fig. 5*A2*), have recently been described as a candidate population of rhythmogenic neurons (Hinckley et al., 2005; Wilson et al., 2005). Although the mouse locomotor network may be quite different from that of the rat, the blockade of I_{NaP} abolishes fictive locomotion in both species (Tazerart et al., 2007b; Zhong et al., 2007). We thus tested the ability of 12 Hb9 cells to generate I_{NaP}-dependent bursting properties. After the membrane was ruptured, the green fluorescent diffusion into the tip of the patch-clamp pipette confirmed that recordings were performed in Hb9 cells (Fig. 5*A2*, insets). $Hb9^+$ interneurons recorded were small with high input resistances (mean, 950 ± 85 MΩ). The most remarkable finding was the strong bursting ability of Hb9 cells in $[Ca^{2+}]_o$-free ACSF (Fig. 5*B2*) (11 of the 12 Hb9 cells), which was abolished by riluzole (10 μM) (Fig. 5*C2*). Among the bursting cells, most of them (10 of 11) displayed pacemaker-like properties (Fig. 5*B2*) with a range of frequencies similar to that of CINs (0.15 ± 0.03 to 0.93 ± 0.13 Hz). Among pacemakers, six were silent at hyperpolarized potentials, whereas the others exhibited signs of electrical coupling with subthreshold membrane oscillations abolished by carbenoxolone (data not shown). In summary, putative locomotor CPGs interneurons have the ability to generate I_{NaP}-dependent bursts in a frequency range quite similar to that of fictive locomotor rhythms.

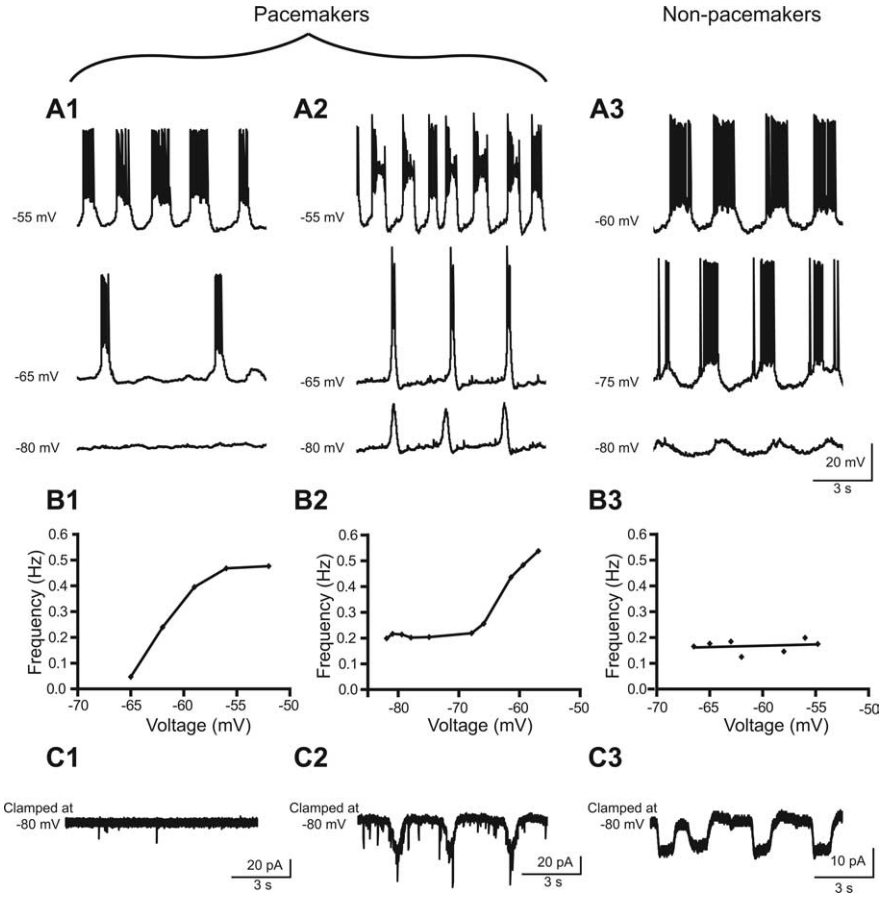

Figure 3. Two types of bursting neurons coexist in the locomotor CPG region. ***A1–A3***, Recurrent bursts induced by incrementing depolarizing current injections in neurons considered as pacemakers (***A1***, ***A2***) or nonpacemakers (***A3***). Pacemakers were subdivided into two groups: those that were silent at hyperpolarized potentials (***A1***) and the others that displayed voltage oscillations at similar potentials (***A2***). ***B1–B3***, Relationship between the frequency of membrane potential oscillations and the holding potential (current-clamp mode) for the neurons illustrated in ***A1–A3***. ***C1–C3***, Current traces of the cells illustrated in ***A*** and voltage clamped at −80 mV.

Table 2. Membrane properties of ventromedial interneurons classified on the basis of their bursting patterns

	Pacemakers	Nonpacemakers
n	36	9
R_m (MΩ)	890 ± 98	495 ± 173
AP amp (mV)	55 ± 1.7	57.8 ± 3.4
AP dur (ms)	2.4 ± 0.1	1.9 ± 0.2
AP threshold (mV)	−45.5 ± 1	−44 ± 3
Rheobase (pA)	16.9 ± 3.7	21.2 ± 5.6

n represents the number of cells. AP, Action potential; amp, amplitude; dur, duration.

Veratridine specifically enhances I_{NaP} and induces intrinsic bursting properties

Effects of an upregulation of I_{NaP} on locomotor activity by variations of $[Ca^{2+}]_o$ would be difficult to identify because Ca^{2+} influences synaptic transmission and electrical properties. The alkaloid veratridine has been described to enhance I_{NaP} (Alkadhi and Tian, 1996) and may thus be used to investigate the role of I_{NaP} in modulating the locomotor activity. Before applying veratridine on fictive locomotor activity, a major issue was to determine its effectiveness to enhance I_{NaP}. Different doses of veratridine from 10 to 240 nM were tested on the amplitude of I_{NaP}. To avoid any masking effects of $[Ca^{2+}]_o$ on the upregulation of I_{NaP}, a voltage-clamp protocol similar to the one used above was performed in normal ACSF (1.2 mM $[Ca^{2+}]_o$) containing the following synaptic blockers: kynurenic acid (1.5 mM), bicuculline (20 μM), and strychnine (1 μM). At 60 nM, veratridine started to significantly increase the amplitude of I_{NaP} on the ascending *I–V* function (+42%; $p < 0.05$, Wilcoxon's paired test; $n = 6$ cells) (Fig. 6*A*). Higher concentrations of veratridine such as 120 and 240 nM increased the amplitude of I_{NaP} by 233% ($p < 0.05$, Wilcoxon's paired test; $n = 7$ cells) (Fig. 6*A*) and 302% ($p < 0.05$, Wilcoxon's paired test; $n = 6$ cells) (Fig. 6*A*), respectively. Thus, the concentration used for the following experiments was 60 nM. At this concentration, veratridine was sufficient to induce a leftward shift in the voltage activation threshold of I_{NaP} from −53.5 ± 1 mV to −59 ± 2 ($p < 0.05$, Wilcoxon's paired test) (Fig. 6*B*). However, the most remarkable effects occurred on the descending *I–V* function such that (1) the amplitude of I_{NaP} increased by 190 ± 48% ($p < 0.05$, Wilcoxon's paired test) (Fig. 6*C1*,*C2*) and (2) the voltage at which I_{NaP} turned off became more

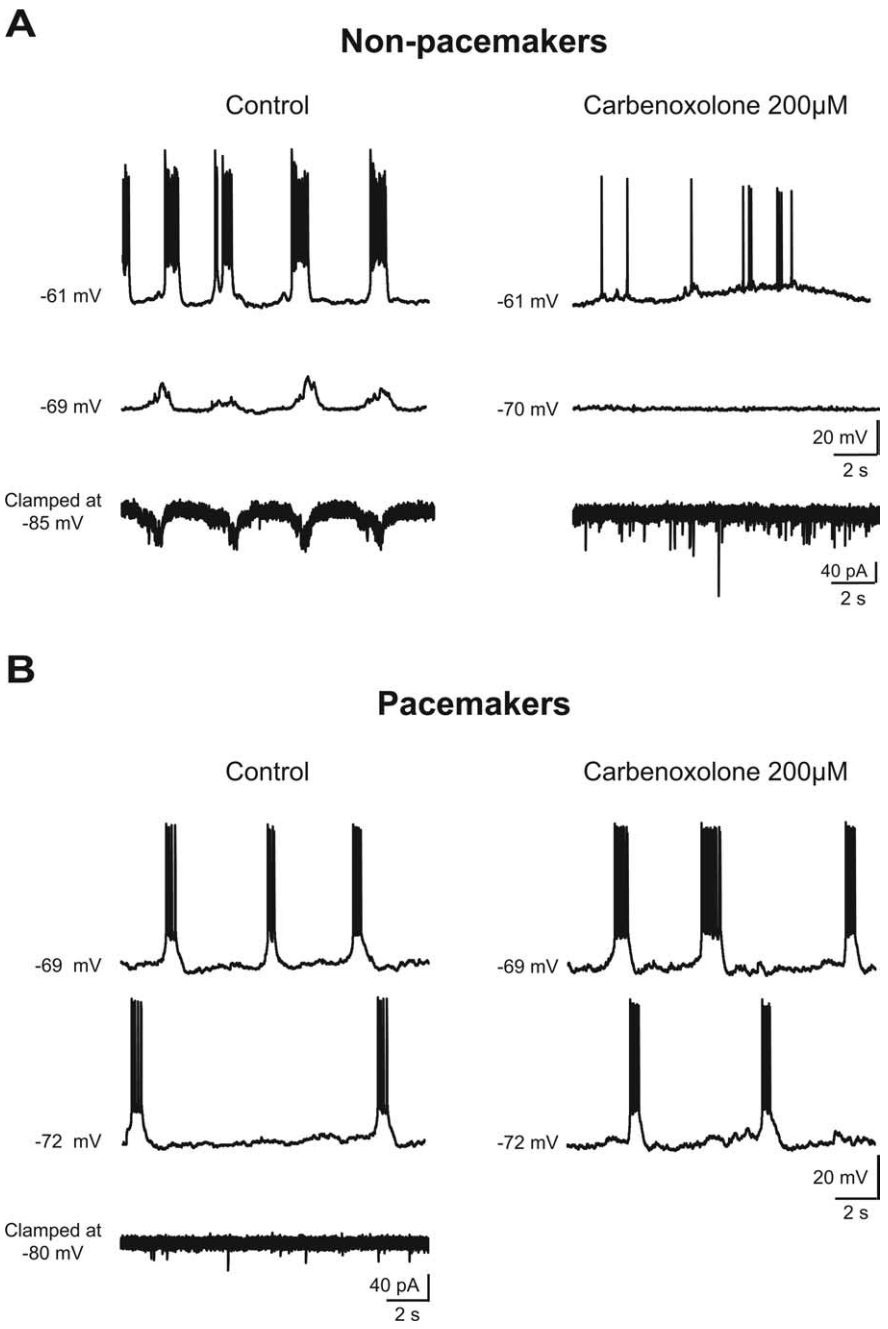

Figure 4. Subthreshold membrane oscillations reflect gap junction-mediated inputs from bursting cells. ***A***, ***B***, Recordings in $[Ca^{2+}]_o$-free ACSF from a nonpacemaker cell (***A***) and a pacemaker cell (***B***) before (right) and 40 min after bath application of carbenoxolone (200 μM; left). In each panel, the top two traces illustrate recordings performed in current-clamp mode at different membrane potentials, whereas the bottom trace illustrates recordings performed in voltage-clamp mode. Membrane potentials are indicated on the left of each trace.

negative (below −70 mV) than its voltage activation threshold (Fig. 6*C1*,*C2*). In other words, veratridine developed a strong hysteresis ("clockwise"), which is known to be a fundamental feature of bistable behavior (Lee and Heckman, 1998; Svirskis and Hounsgaard, 1998). We then investigated the effects of veratridine on the firing properties of 12 ventromedial neurons. All ventromedial interneurons recorded switched their regular-spiking pattern into a bursting mode (Fig. 7*A1*,*A2*), which was disrupted by riluzole (10 μM) (Fig. 7*A3*). Veratridine-induced bursts differed from those described above in $[Ca^{2+}]_o$-free ACSF; they had a longer duration (15 ± 1.5 s) and were generated at a low frequency (0.026 ± 0.004 Hz), which was relatively insensitive to the amount of injected current. In line with some of these observations, bursts induced in $[Ca^{2+}]_o$-free ACSF with a near-threshold depolarization in five cells, were significantly increased in duration (from 1.7 ± 0.2 to 9.6 ± 1.4 s; $p < 0.05$, Wilcoxon's paired test) (Fig. 7*B1*,*B2*) and decreased in frequency (from 0.15 ± 0.03 to 0.05 ± 0.015 Hz; $p < 0.05$, Wilcoxon's paired test) (Fig. 7*B1*,*B2*) by veratridine. Analyzing the voltage responses to subthreshold current pulses revealed that veratridine altered neither the input resistance nor the holding membrane potential ($p > 0.05$, Wilcoxon's paired test) (Table 3) (Fig. 7*A*, dotted line). Amplitude, duration, and threshold of the spike as well as the rheobase (minimum current required to trigger it) were unchanged by veratridine ($p > 0.05$, Wilcoxon's paired test) (Table 3). Possible effects on synaptic transmission were also investigated by comparing mEPSCs and mIPSCs before and after the application of veratridine (Fig. 8*A1*,*B1*). Neither the amplitudes (Fig. 8*A2*,*B2*, Table 3) nor the frequencies of mEPSCs and mIPSCs (Table 3), measured at a holding potential of −70 mV, were affected by veratridine.

To conclude, 60 nM veratridine selectively enhanced I_{NaP} and induced intrinsic bursting properties without affecting the membrane properties of neurons and the synaptic transmission within the spinal cord. In the next step of our investigation, we therefore used this tool to test the effect of a modulation of I_{NaP} on the operation of the spinal cord locomotor networks.

Veratridine slows down the locomotor rhythm

In the neonatal rat, rostral lumbar segments (L1/L2) have a greater capacity to express locomotor-like activity than the caudal ones (Cazalets et al., 1995). A Vaseline barrier was built at the L2/L3 level to superfuse the most important part of the locomotor CPG independently from the motoneurons recorded at the L5 level (Fig. 9). In seven isolated spinal cord preparations, NMA/5-HT (15 μM/5 μM) was first bath applied in both pools to induce a locomotor-like activity (Fig. 9*A1*). The cycle periods were initially long and shortened progressively until a steady state was reached within 5 min (data not shown). This steady-state activity was analyzed over a 5 min time window (see characteristics in Table 4). After washout, a second application of NMA/5-HT was performed and veratridine was added rostral to the barrier (Fig. 9*A2*). The cycle period and burst duration significantly increased by 37 ± 14 and 61 ± 16%, respectively ($p < 0.05$, Wilcoxon's paired test) (Table 4). No apparent effect on burst amplitude was observed (103 ± 10% of the control; $p >$

0.05, Wilcoxon's paired test) (Table 4). However, a concomitant decrease of cross-correlation values occurred ($p > 0.05$, Wilcoxon's paired test) (Table 4). Rather than a disruption of the left/right alternation, this decrease may result from the increase in burst duration induced by veratridine thereby causing an overlap of opposite ventral root bursts (Fig. 9*A2*). Effects of veratridine on fictive locomotion were not reversible after a 2 h washout (data not shown).

To confirm that the effects on fictive locomotion resulted from a specific increase of I_{NaP} rather than from a desensitization of the spinal cord after successive applications of NMA/5-HT, a second series of experiments ($n = 4$) was performed with two consecutive applications of NMA/5-HT alone (Fig. 9*B*). The characteristics of the fictive locomotor activity (period, burst duration and amplitude, cross-correlation coefficient) were similar for the two applications (Table 5). Together, our results demonstrate that a specific upregulation of I_{NaP} at the CPG level slowed down the locomotor rhythm.

Discussion

We provide evidence that, in addition to generating pacemaker properties in locomotor CPG interneurons, an upregulation of the I_{NaP} slows the locomotor rhythm down. These findings pave the way for a new working hypothesis in which I_{NaP}-dependent pacemaker neurons play a key role in locomotor rhythm generation.

I_{NaP} enables the expression of pacemaker properties in putative CPG interneurons

Bursting properties are determined by intrinsic membrane properties because they persisted after blocking chemical and electrical synaptic transmissions. They are independent of both voltage-sensitive Ca^{2+} channels (blocked by cadmium) and intracellular Ca^{2+} stores (chelation of Ca^{2+}). Our observations support a primary role for I_{NaP} in bursting properties. First, lumbar ventromedial interneurons displayed an I_{NaP} (Tazerart et al., 2007b; Theiss et al., 2007; Zhong et al., 2007). Second, the depolarization leading to bursts occurred at a voltage close to the I_{NaP} threshold. Third, the ability to burst developed in parallel with an upregulation of I_{NaP}. Fourth, TTX or riluzole disrupted bursting properties before affecting spikes.

TTX-resistant oscillatory properties have been investigated in rodent lumbar spinal cord. They are conditional because they were evoked by excitatory amino acid agonists (MacLean et al., 1997; Schmidt et al., 1998; Tresch and Kiehn, 2000) and/or neuromodulators (Wilson et al., 2005; Han et al., 2007). In the absence of neurotransmitters, we provide the demonstration of TTX-sensitive oscillatory properties that exhibited one of the main characteristics of pacemakers (i.e., the voltage dependency of their frequency). In their modeling study, McCrea and Rybak (2007) have postulated that I_{NaP} can function as a primary voltage-dependent mechanism to generate the locomotor rhythm. We provide the first physiological evidence for the existence of such bursting cells in the core of the locomotor CPG. Only cells with a large I_{NaP} are likely able to express bursts. In the pre-Bötzinger complex, bursting neurons have a larger ratio of I_{NaP} over leak conductances than nonbursting cells (Del Negro et al., 2002; Koizumi and Smith, 2008).

Hb9 interneurones fulfill most of criteria necessary for rhythm-generating neurons (Brownstone and Wilson, 2008). Al-

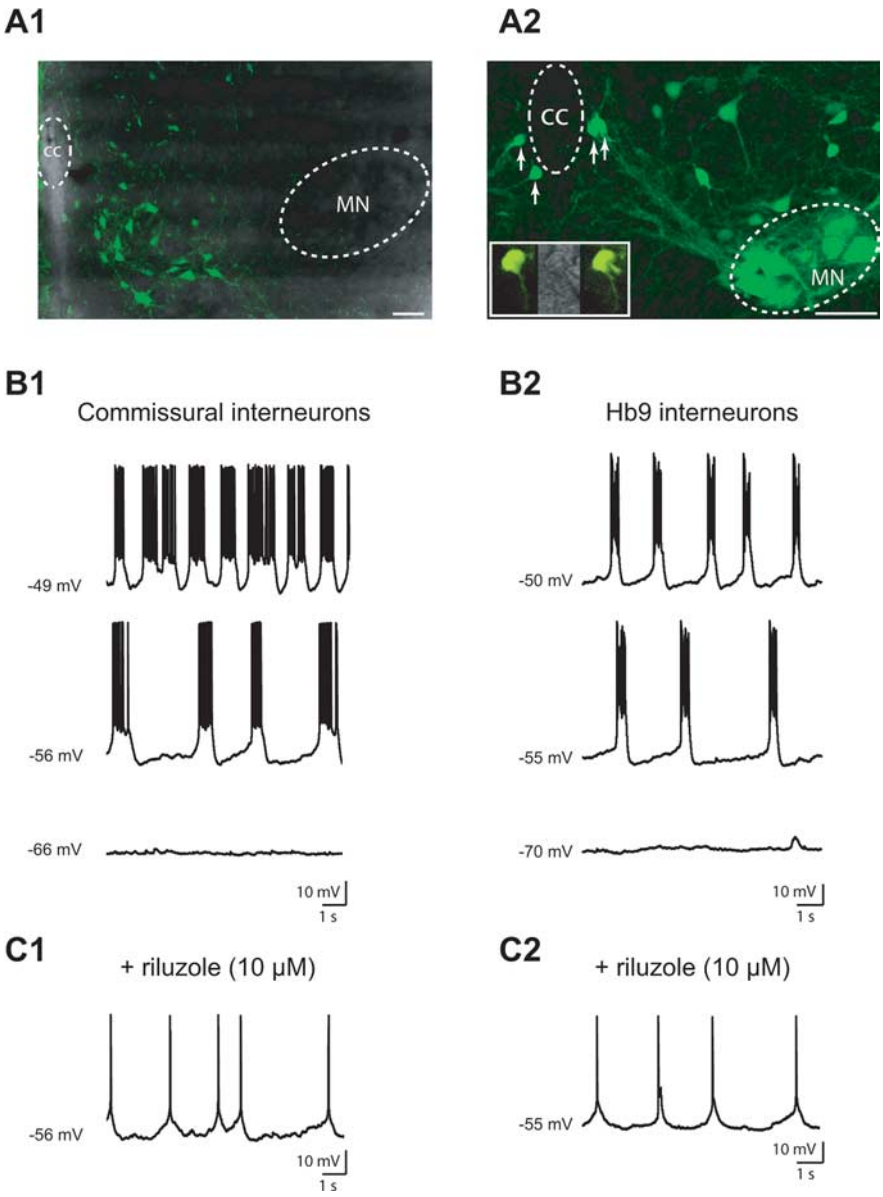

Figure 5. Interneurons considered to be part of the locomotor CPG express I_{NaP}-dependent bursting properties. ***A1***, ***A2***, Confocal projection images in the ventral part of upper lumbar segments showing the organization of dextran-labeled commissural interneurons (***A1***) and GFP^+ neurones (***A2***) from the neonatal rat and the Hb9:eGFP transgenic mice, respectively. The dashed circles highlight the limits of both the central canal (CC) and the motoneuronal pool (MN). The arrows in ***A2*** show bilaterally located GFP^+ neurones targeted as putative Hb9 cells. Scale bars, 50 μm. The insets in ***A2*** illustrate a GFP^+ interneuron patch clamped under infrared-differential interference contrast. The GFP diffusion into the patch-clamp pipette confirmed that recordings were performed from GFP^+ interneurons. ***B1***, ***B2***, Recurrent bursts induced by incrementing depolarizing currents in a descending commissural interneuron (***B1***) and in a Hb9 interneuron (***B2***) both recorded in $[Ca^{2+}]_o$-free ACSF. ***C1***, ***C2***, Same cells as in ***B*** 15 min after the application of riluzole (10 μM). Membrane potentials are mentioned on the left of each trace.

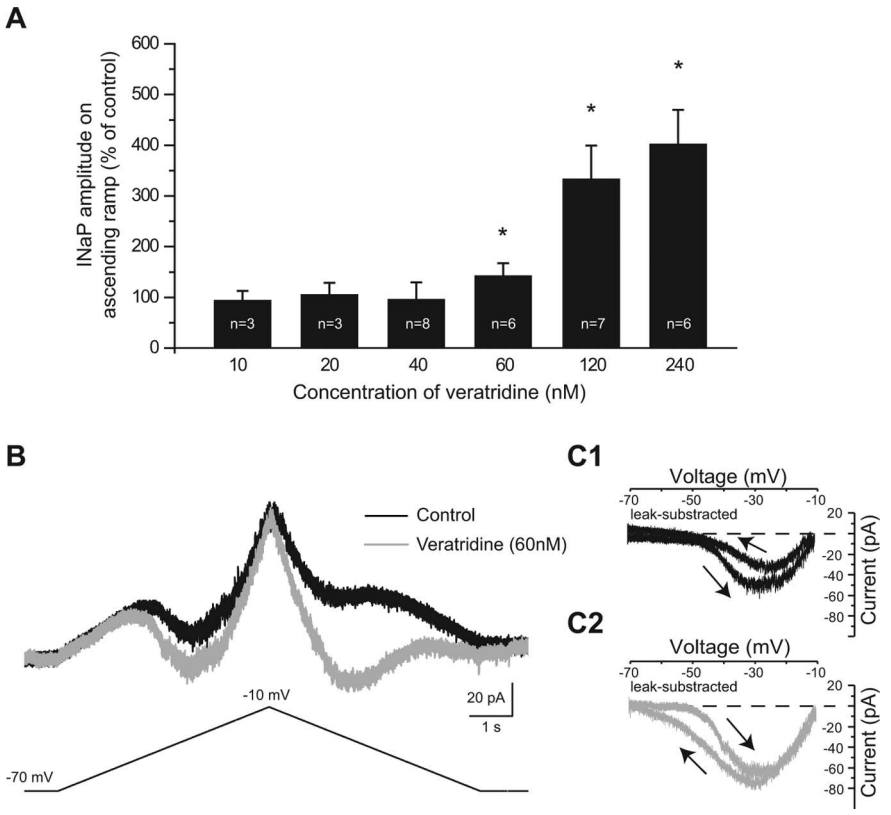

Figure 6. Effects of veratridine on biophysical properties of I_{NaP}. ***A***, Effect of different concentrations of veratridine (from 10 to 240 nM) on the peak amplitude of the I_{NaP} measured on the ascending voltage ramp. *n*, Number of cells recorded. Error bars indicate SEM. $*p < 0.05$. Statistical significance was assessed by a Wilcoxon paired test. ***B***, Total membrane current (top traces) evoked by triangular voltage ramps (bottom trace) from −70 to +10 mV and back to −70 mV over 10 s, before (black trace) and after the application of 60 nM veratridine (dark gray trace). ***C1***, ***C2***, Same current leak-subtracted and plotted as a function of command voltage before (***C1***) and after the application of 60 nM veratridine (***C2***). The arrows indicate direction of voltage changes.

Table 3. Absence of side effects of 60 nM veratridine on membrane properties and synaptic transmission of ventromedial interneurons

	Control	Veratridine (60 nM)
Membrane properties ($n = 8$)		
Input resistance (MΩ)	1050 ± 187	1054 ± 226
Membrane potential (mV)	−63.9 ± 2.3	−64.6 ± 2.9
Spike duration (ms)	1.91 ± 0.07	1.94 ± 0.07
Spike amplitude (mV)	50.5 ± 3.1	49.5 ± 2.3
Spike threshold (mV)	−50.7 ± 1.6	−51.9 ± 2.1
Rheobase (pA)	18.5 ± 3.7	19.9 ± 3.2
Synaptic transmission ($n = 7$)		
mEPSCs amplitude (pA)	23.8 ± 2.3	23.3 ± 2.3
mEPSCs interval (ms)	859 ± 183	809 ± 124
mIPSCs amplitude (pA)	45.7 ± 5.7	45.3 ± 4.9
mIPSCs interval (ms)	1362 ± 455	1366 ± 362

n represents the number of cells. Statistical significance was assessed by a Wilcoxon paired test.

Table 4. Effects of veratridine (60 nM) on the parameters of fictive locomotion

	Control	Veratridine (60 nM)
n	7	7
Burst amplitude (%)	100 ± 10	103 ± 10
Burst duration (s)	2.5 ± 0.2	3.4 ± 0.3*
Cycle period (s)	1.35 ± 0.13	2.2 ± 0.2*
Cross-correlation coefficient	0.58 ± 0.03	0.46 ± 0.03*

n represents the number of preparations.

$*p < 0.05$. Statistical significance was assessed by a Wilcoxon paired test.

though electrical coupling between Hb9 cells is somewhat controversial (Wilson et al., 2008; Ziskind-Conhaim and Hinckley, 2008), they seem to be coupled with GFP-positive interneurons that do not express the Hb9 protein (Wilson et al., 2007). Some of our bursting Hb9 cells exhibited signs of electrical coupling with subthreshold membrane oscillations. It is possible that "false" Hb9 interneurons display I_{NaP}-dependent bursting properties to form a pacemaker group of heterogeneous interneurons that may be critical to locomotor rhythm generation. Only descending CINs were investigated without discriminating between those whose axons turn caudally after crossing the midline (dCINs) and those whose axons bifurcate after crossing the midline (adCINs). In contrast to dCINs, adCINs do not fire rhythmically during fictive locomotion, suggesting that they do not belong to the locomotor CPG (Zhong et al., 2006b). Because only one-half of the recorded CINs displayed bursts, it will be interesting to determine whether bursting properties are exclusive to dCINs.

Role of gap junction coupling

Our results suggest that most, if not all, bursting cells are electrically coupled to each other. This is consistent with the physiological evidence of electrical synapses between locomotor-related interneurons (Hinckley and Ziskind-Conhaim, 2006; Zhong et al., 2006a; Wilson et al., 2007). Modeling studies predict a rhythmogenic role for electrical synapses such that coupling between nonpacemaker cells leads to bursting (Smolen et al., 1993; Skinner et al., 1999). In our study, this emergent property does not appear to be the primary mechanism underlying bursting. Pacemaker cells, by far the most representative type of bursting cells, were indeed not affected under carbenoxolone. Because of the large proportion of pacemaker cells, bursting neurons without pacemaker properties are likely "follower" neurons. In summary, rather than a rhythmogenic function, our data support the classical view that gap junction coupling is mainly required for synchronizing activities (Bennett and Zukin, 2004).

Modulation of the I_{NaP} and consequences on bursting properties

An intriguing observation was the relationship between bursting activity and $[Ca^{2+}]_o$. As described in the hippocampus (Su et al., 2001), lowering $[Ca^{2+}]_o$ increased the propensity of neurons to burst. The AHP is dominated by a Ca^{2+}-activated K^+ conductance and thereby abolished by the removal of $[Ca^{2+}]_o$. A switch from spiking to bursting has been reported after blocking Ca^{2+}-activated K^+ channels (Cingolani et al., 2002). Although ventromedial interneurons display a prominent AHP (Tazerart et al., 2007b), its blockade by apamin did not generate bursts. Therefore, the limitation of burst firing by $[Ca^{2+}]_o$ did not occur through a modulation of the AHP. One mechanism operating in the generation of bursts by $[Ca^{2+}]_o$ involves enhancement of I_{NaP}. As previously observed in supraoptic (Li and Hatton, 1996)

and CA1 pyramidal cells (Yue et al., 2005), we found that $[Ca^{2+}]_o$-free ACSF shifts I_{NaP} activation threshold to more negative potentials and enhances its amplitude. $[Ca^{2+}]_o$ has been proposed to stabilize both ionic pores within membrane and screen charges in the vicinity of the plasma membrane (Bertil Hille, 2001). A reduction in $[Ca^{2+}]_o$ may thus increase the availability of negative surface charges on the outside of the cell, which in turn could facilitate Na^+ influx (Xiong et al., 1997).

Moderate concentrations of veratridine produced a similar leftward shift of the I_{NaP} activation threshold than that described after removing $[Ca^{2+}]_o$. This is consistent with veratridine-modified channels that activate at more hyperpolarized voltages (Leibowitz et al., 1986). However, the most conspicuous change with veratridine was the marked enlargement of the current seen during the decay phase of the voltage ramps. This change should be principally ascribed to a slow deactivation process that gives rise to a hysteretic current. The slowed deactivation counteracts repolarization and therefore makes ventromedial interneurons burst with longer-lasting discharge. Small concentrations of veratridine enabled bursting without noticeable effect on synaptic transmission and membrane properties (Alkadhi and Tian, 1996).

These results suggest that there is a direct relationship between the strength of I_{NaP} and the tendency of the cells to burst. The shift of I_{NaP} activation toward more hyperpolarizing values may be required to initiate bursts, whereas regulation of the deactivation kinetics may play an important role in controlling burst duration, as suggested by the observation that veratridine increased burst duration in $[Ca^{2+}]_o$-free ACSF. Thus, although additional investigations are needed to identify mechanisms for burst repolarization, regulation of the biophysical properties of I_{NaP} seems to contribute (Butera et al., 1999; Del Negro et al., 2002). The Na^+/K^+ electrogenic pump (Ballerini et al., 1997; Darbon et al., 2003), the Na^+-dependent K^+ current (Schwindt et al., 1989), the glial KCl accumulation (Bikson et al., 1999), and slow activation of K^+ currents (Yue and Yaari, 2004) might also regulate the burst repolarization process. It should be noted that the emergence of subthreshold oscillations in $[Ca^{2+}]_o$-free ACSF unlikely results only from the modulation of I_{NaP} because they were not induced by veratridine. More likely, a concomitant increase of electrical coupling may be responsible for subthreshold oscillations. Lowering $[Ca^{2+}]_o$ has indeed been reported to also increase gap junctional communication (Perez-Velazquez et al., 1994). Thus, beside the primary role of I_{NaP} in generating bursts, other changes in Ca^{2+}-dependent membrane properties may be involved.

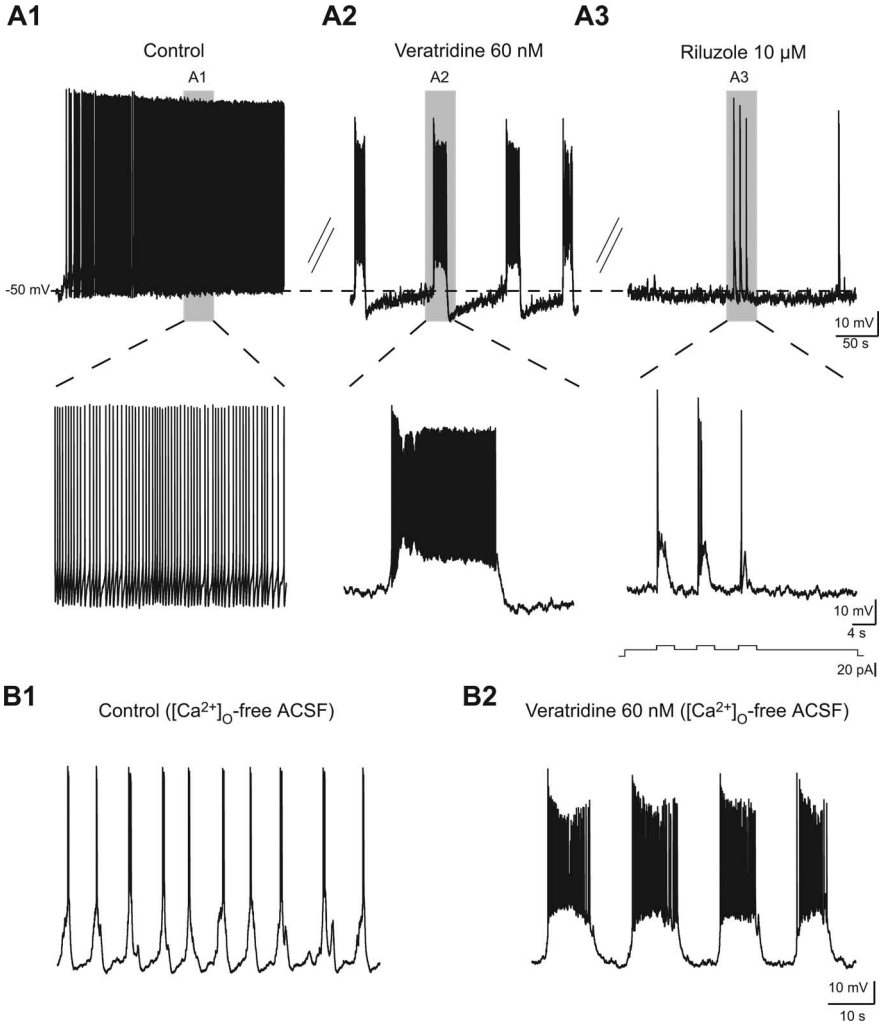

Figure 7. Veratridine-enhanced I_{NaP} induces bursting properties. ***A1–A3***, Voltage traces of a ventromedial interneuron recorded in 1.2 mM $[Ca^{2+}]_o$ before (***A1***) and after (***A2***) the application of 60 nM veratridine. A subsequent application of riluzole (10 μM) abolished bursts without affecting spikes generated by brief current pulses (***A3***, bottom trace). The shaded areas are shown at a faster timescale in ***A1–A3***. The dotted line illustrates the level of the membrane potential at −50 mV. ***B1***, ***B2***, Voltage traces of a ventromedial interneuron recorded in $[Ca^{2+}]_o$-free ACSF before (***B1***) and after the application of 60 nM veratridine (***B2***).

Table 5. Effects of two consecutive applications of NMA/5-HT on the parameters of fictive locomotion

	First application	Second application
n	4	4
Burst amplitude (%)	100 ± 5	94.4 ± 2.6
Burst duration (s)	1.3 ± 0.08	1.2 ± 0.06
Cycle period (s)	2.4 ± 0.2	2.2 ± 0.1
Cross-correlation coefficient	0.58 ± 0.05	0.55 ± 0.06

n represents the number of preparations.

Functional considerations

The ionic mechanisms underlying burst generation in this study are quite different from the sodium-independent currents previously described in "conditional" bursters of the locomotor CPG (Hochman et al., 1994; Kiehn et al., 1996; Wilson et al., 2005). We describe a second type of bursting property, dependent on I_{NaP}, making the pacemaker abilities in the locomotor CPG heterogeneous. Two types of respiratory pacemaker neurons have been found based on the activation of I_{NaP} and calcium-activated nonspecific cationic current, respectively (Thoby-Brisson and Ramirez, 2001; Del Negro et al., 2005). Both are essential to sustain fast respiratory rhythm during eupnea, whereas I_{NaP}-dependent pacemaker cells alone are sufficient to generate slow respiratory rhythm for gasping (Peña et al., 2004; Ramirez et al.,

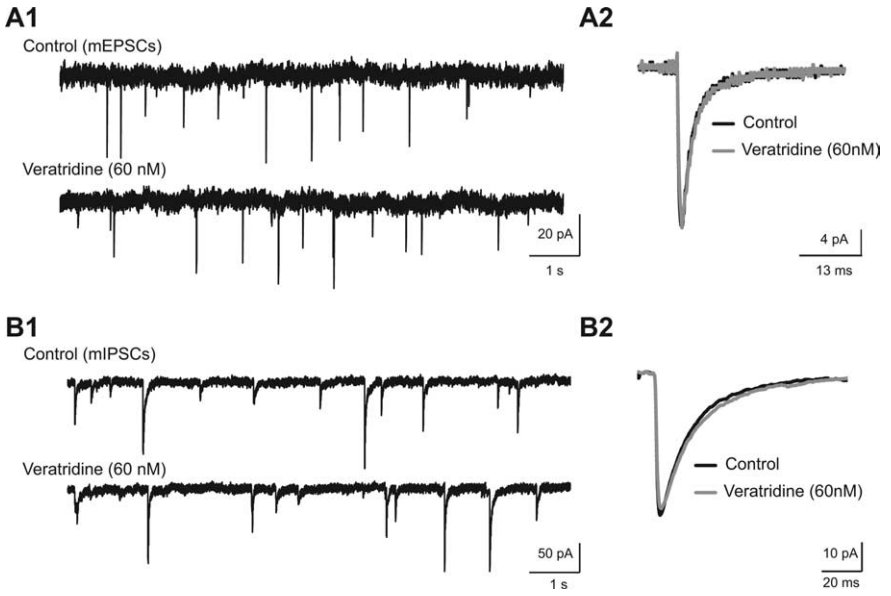

Figure 8. Absence of side effects of 60 nM veratridine on synaptic transmission. ***A1–B2***, Effects of veratridine on mEPSCs (***A***) and mIPSCs (***B***) in ventromedial interneurons. ***A1***, ***B1***, Traces of continuously recorded mEPSCs (***A1***) and mIPSCs (***B1***) in a ventromedial interneuron voltage clamped at −70 mV before (top trace) and 20 min after adding 60 nM veratridine (bottom trace). ***A2***, ***B2***, Averaged mEPSCs (***A2***) and mIPSCs (***B2***) recorded before and 20 min after adding veratridine.

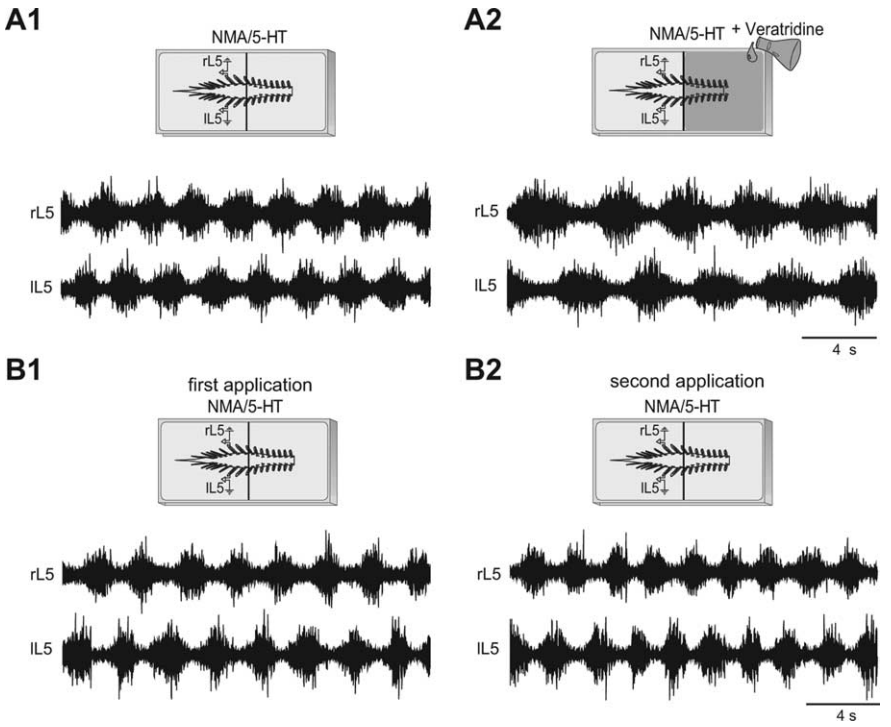

Figure 9. Veratridine slows down the locomotor rhythm. ***A1***, ***B2***, Locomotor-like activity during bath application of NMA/5-HT (15 μM/5 μM) in both compartments before (***A1***) and after adding veratridine to rostral lumbar segments (***A2***). Raw recordings are collected from opposite ventral roots (IL5 and rL5). ***B1***, ***B2***, Locomotor-like activity during the first (***B1***) and the second (***B2***) bath application of NMA/5-HT (15 μM/5 μM) in both compartments. The diagrams in ***A*** and ***B*** illustrate the experimental paradigm. A Vaseline barrier was built at the L2/L3 level to superfuse the most important part of the locomotor CPG independently from the motoneurons recorded from opposite L5 ventral roots.

2004). As for the respiratory system, we assume that the relative contribution of bursting modes may be regulated to adapt the rhythmic locomotor output to ongoing needs.

Reducing $[Ca^{2+}]_o$ upregulated I_{NaP} and induced bursts within a frequency range well matched with *in vitro* locomotor rhythms. Under resting conditions, the $[Ca^{2+}]_o$ in rat CSF is ~1.6 and ~1.2 mM in the fetus and adult, respectively (Jones and Keep, 1988). Of special interest, reductions in $[Ca^{2+}]_o$ accompany neuronal activity in cortical networks (Pumain and Heinemann, 1981; Amzica et al., 2002). We expect that similar changes of $[Ca^{2+}]_o$ occur in the microenvironment of locomotor CPG when active. It follows that enhanced I_{NaP} may generate bursting properties in Hb9 interneurons to promote locomotor rhythm. This hypothesis is based on a previous report showing that locomotor activity relies on I_{NaP} (Tazerart et al., 2007b; Zhong et al., 2007) and that rhythm emanates from ipsilaterally projecting glutamatergic excitatory interneurons (Kiehn, 2006) similar to Hb9 cells (Hinckley et al., 2005; Wilson et al., 2005). However, the efficacy of electrotonic coupling is also increased by lowering $[Ca^{2+}]_o$ (Perez-Velazquez et al., 1994). Electrical synapses would be particularly suited to synchronize the bursting of CPG interneurons (Tresch and Kiehn, 2000). By modulating both I_{NaP} and gap junctions, changes in $[Ca^{2+}]_o$ may represent a fast and powerful mechanism to regulate the operation of the locomotor CPG.

A specific upregulation of I_{NaP} slowed down the locomotor rhythm. Monoamines have similar effects (Sqalli-Houssaini et al., 1993; Kiehn and Kjaerulff, 1996; Barrière et al., 2004; Pearlstein et al., 2005). 5-HT and dopamine excite commissural interneurons (Carlin et al., 2006; Zhong et al., 2006a,b) and Hb9 cells (Han et al., 2007). Considering the ability of 5-HT and dopamine to upregulate I_{NaP} (Gorelova and Yang, 2000; Harvey et al., 2006), the neuromodulation of I_{NaP} might play a key role in the dynamic reconfiguration of the locomotor network by regulating bursting properties of pacemaker cells. In addition to the upregulation of I_{NaP}, the ability to burst may also rely on the facilitation of I_{NaP} via a reduction of opposing outward K^+ currents (Purvis et al., 2007; Koizumi and Smith, 2008) and/or a direct facilitation of L-type calcium channels involved in bistable properties (Svirskis and Hounsgaard, 1998).

The description of a new I_{NaP}-dependent bursting property makes the pacemaker network hypothesis a valuable model to account for locomotor rhythm generation. We conclude that the pacemaker network property acts in concert with the emergent-network mechanisms to adapt the rhythmic patterned motor output to ongoing needs (Rybak et al., 2006; Kozlov et al., 2007; Purvis et al., 2007).

References

Alkadhi KA, Tian LM (1996) Veratridine-enhanced persistent sodium current induces bursting in CA1 pyramidal neurons. Neuroscience 71:625–632.

Amzica F, Massimini M, Manfridi A (2002) Spatial buffering during slow and paroxysmal sleep oscillations in cortical networks of glial cells *in vivo*. J Neurosci 22:1042–1053.

Arshavsky YI (2003) Cellular and network properties in the functioning of the nervous system: from central pattern generators to cognition. Brain Res Rev 41:229–267.

Azouz R, Alroy G, Yaari Y (1997) Modulation of endogenous firing patterns by osmolarity in rat hippocampal neurones. J Physiol 502:175–187.

Ballerini L, Bracci E, Nistri A (1997) Pharmacological block of the electrogenic sodium pump disrupts rhythmic bursting induced by strychnine and bicuculline in the neonatal rat spinal cord. J Neurophysiol 77:17–23.

Barrière G, Mellen N, Cazalets JR (2004) Neuromodulation of the locomotor network by dopamine in the isolated spinal cord of newborn rat. Eur J Neurosci 19:1325–1335.

Bennett MV, Zukin RS (2004) Electrical coupling and neuronal synchronization in the mammalian brain. Neuron 41:495–511.

Bertil Hille (2001) Ion channels of excitable membranes. Sunderland, MA: Sinauer.

Bikson M, Ghai RS, Baraban SC, Durand DM (1999) Modulation of burst frequency, duration, and amplitude in the zero-Ca^{2+} model of epileptiform activity. J Neurophysiol 82:2262–2270.

Brocard F, Vinay L, Clarac F (1999) Gradual development of the ventral funiculus input to lumbar motoneurons in the neonatal rat. Neuroscience 90:1543–1554.

Brocard F, Verdier D, Arsenault I, Lund JP, Kolta A (2006) Emergence of intrinsic bursting in trigeminal sensory neurons parallels the acquisition of mastication in weanling rats. J Neurophysiol 96:2410–2424.

Brownstone RM, Wilson JM (2008) Strategies for delineating spinal locomotor rhythm-generating networks and the possible role of Hb9 interneurones in rhythmogenesis. Brain Res Rev 57:64–76.

Butera RJ Jr, Rinzel J, Smith JC (1999) Models of respiratory rhythm generation in the pre-Botzinger complex. I. Bursting pacemaker neurons. J Neurophysiol 82:382–397.

Butt SJ, Kiehn O (2003) Functional identification of interneurons responsible for left-right coordination of hindlimbs in mammals. Neuron 38:953–963.

Carlin KP, Dai Y, Jordan LM (2006) Cholinergic and serotonergic excitation of ascending commissural neurons in the thoraco-lumbar spinal cord of the neonatal mouse. J Neurophysiol 95:1278–1284.

Cazalets JR, Borde M, Clarac F (1995) Localization and organization of the central pattern generator for hindlimb locomotion in newborn rat. J Neurosci 15:4943–4951.

Cazalets JR, Sqalli-Houssaini Y, Magoul R (1999) Differential effects of potassium channel blockers on the activity of the locomotor network in neonatal rat. Brain Res 827:185–197.

Cingolani LA, Gymnopoulos M, Boccaccio A, Stocker M, Pedarzani P (2002) Developmental regulation of small-conductance Ca^{2+}-activated K^+ channel expression and function in rat Purkinje neurons. J Neurosci 22:4456–4467.

Crill WE (1996) Persistent sodium current in mammalian central neurons. Annu Rev Physiol 58:349–362.

Darbon P, Tscherter A, Yvon C, Streit J (2003) Role of the electrogenic Na/K pump in disinhibition-induced bursting in cultured spinal networks. J Neurophysiol 90:3119–3129.

Darbon P, Yvon C, Legrand JC, Streit J (2004) I_{NaP} underlies intrinsic spiking and rhythm generation in networks of cultured rat spinal cord neurons. Eur J Neurosci 20:976–988.

Del Negro CA, Koshiya N, Butera RJ Jr, Smith JC (2002) Persistent sodium current, membrane properties and bursting behavior of pre-Botzinger complex inspiratory neurons in vitro. J Neurophysiol 88:2242–2250.

Del Negro CA, Morgado-Valle C, Hayes JA, Mackay DD, Pace RW, Crowder EA, Feldman JL (2005) Sodium and calcium current-mediated pacemaker neurons and respiratory rhythm generation. J Neurosci 25:446–453.

Gao BX, Stricker C, Ziskind-Conhaim L (2001) Transition from GABAergic to glycinergic synaptic transmission in newly formed spinal networks. J Neurophysiol 86:492–502.

Gorelova NA, Yang CR (2000) Dopamine D1/D5 receptor activation modulates a persistent sodium current in rat prefrontal cortical neurons in vitro. J Neurophysiol 84:75–87.

Grillner S (2006) Biological pattern generation: the cellular and computational logic of networks in motion. Neuron 52:751–766.

Han P, Nakanishi ST, Tran MA, Whelan PJ (2007) Dopaminergic modulation of spinal neuronal excitability. J Neurosci 27:13192–13204.

Harvey PJ, Li X, Li Y, Bennett DJ (2006) 5-HT2 receptor activation facilitates a persistent sodium current and repetitive firing in spinal motoneurons of rats with and without chronic spinal cord injury. J Neurophysiol 96:1158–1170.

Hinckley CA, Ziskind-Conhaim L (2006) Electrical coupling between locomotor-related excitatory interneurons in the mammalian spinal cord. J Neurosci 26:8477–8483.

Hinckley CA, Hartley R, Wu L, Todd A, Ziskind-Conhaim L (2005) Locomotor-like rhythms in a genetically distinct cluster of interneurons in the mammalian spinal cord. J Neurophysiol 93:1439–1449.

Hochman S, Jordan LM, MacDonald JF (1994) *N*-Methyl-D-aspartate receptor-mediated voltage oscillations in neurons surrounding the central canal in slices of rat spinal cord. J Neurophysiol 72:565–577.

Hsiao CF, Del Negro CA, Trueblood PR, Chandler SH (1998) Ionic basis for serotonin-induced bistable membrane properties in guinea pig trigeminal motoneurons. J Neurophysiol 79:2847–2856.

Jones HC, Keep RF (1988) Brain fluid calcium concentration and response to acute hypercalcaemia during development in the rat. J Physiol 402:579–593.

Kiehn O (2006) Locomotor circuits in the mammalian spinal cord. Annu Rev Neurosci 29:279–306.

Kiehn O, Kjaerulff O (1996) Spatiotemporal characteristics of 5-HT and dopamine-induced rhythmic hindlimb activity in the in vitro neonatal rat. J Neurophysiol 75:1472–1482.

Kiehn O, Johnson BR, Raastad M (1996) Plateau properties in mammalian spinal interneurons during transmitter-induced locomotor activity. Neuroscience 75:263–273.

Kjaerulff O, Kiehn O (1996) Distribution of networks generating and coordinating locomotor activity in the neonatal rat spinal cord *in vitro*: a lesion study. J Neurosci 16:5777–5794.

Koizumi H, Smith JC (2008) Persistent Na^+ and K^+-dominated leak currents contribute to respiratory rhythm generation in the pre-Botzinger complex *in vitro*. J Neurosci 28:1773–1785.

Kozlov AK, Lansner A, Grillner S, Kotaleski JH (2007) A hemicord locomotor network of excitatory interneurons: a simulation study. Biol Cybern 96:229–243.

Lee RH, Heckman CJ (1998) Bistability in spinal motoneurons in vivo: systematic variations in persistent inward currents. J Neurophysiol 80:583–593.

Leibowitz MD, Sutro JB, Hille B (1986) Voltage-dependent gating of veratridine-modified Na channels. J Gen Physiol 87:25–46.

Li Z, Hatton GI (1996) Oscillatory bursting of phasically firing rat supraoptic neurones in low-Ca^{2+} medium: Na^+ influx, cytosolic Ca^{2+} and gap junctions. J Physiol 496:379–394.

MacLean JN, Schmidt BJ, Hochman S (1997) NMDA receptor activation triggers voltage oscillations, plateau potentials and bursting in neonatal rat lumbar motoneurons in vitro. Eur J Neurosci 9:2702–2711.

Madriaga MA, McPhee LC, Chersa T, Christie KJ, Whelan PJ (2004) Modulation of locomotor activity by multiple 5-HT and dopaminergic receptor subtypes in the neonatal mouse spinal cord. J Neurophysiol 92:1566–1576.

McCrea DA, Rybak IA (2007) Modeling the mammalian locomotor CPG: insights from mistakes and perturbations. In: Progress in brain research computational neuroscience: theoretical insights into brain function (Cisek P, Drew T, Kalaska JF, eds), pp 235–253. Amsterdam: Elsevier.

Pape HC (1996) Queer current and pacemaker: the hyperpolarization-activated cation current in neurons. Annu Rev Physiol 58:299–327.

Pearlstein E, Mabrouk FB, Pflieger JF, Vinay L (2005) Serotonin refines the locomotor-related alternations in the in vitro neonatal rat spinal cord. Eur J Neurosci 21:1338–1346.

Peña F, Parkis MA, Tryba AK, Ramirez JM (2004) Differential contribution of pacemaker properties to the generation of respiratory rhythms during normoxia and hypoxia. Neuron 43:105–117.

Perez-Velazquez JL, Valiante TA, Carlen PL (1994) Modulation of gap junctional mechanisms during calcium-free induced field burst activity: a

possible role for electrotonic coupling in epileptogenesis. J Neurosci 14:4308–4317.
Pumain R, Heinemann U (1981) Extracellular calcium and potassium changes in mammalian neocortex. Adv Biochem Psychopharmacol 29:53–58.
Purvis LK, Smith JC, Koizumi H, Butera RJ (2007) Intrinsic bursters increase the robustness of rhythm generation in an excitatory network. J Neurophysiol 97:1515–1526.
Ramirez JM, Tryba AK, Peña F (2004) Pacemaker neurons and neuronal networks: an integrative view. Curr Opin Neurobiol 14:665–674.
Rybak IA, Shevtsova NA, Lafreniere-Roula M, McCrea DA (2006) Modelling spinal circuitry involved in locomotor pattern generation: insights from deletions during fictive locomotion. J Physiol 577:617–639.
Schmidt BJ, Hochman S, MacLean JN (1998) NMDA receptor-mediated oscillatory properties: potential role in rhythm generation in the mammalian spinal cord. Ann N Y Acad Sci 860:189–202.
Schwindt PC, Spain WJ, Crill WE (1989) Long-lasting reduction of excitability by a sodium-dependent potassium current in cat neocortical neurons. J Neurophysiol 61:233–244.
Skinner FK, Zhang L, Velazquez JL, Carlen PL (1999) Bursting in inhibitory interneuronal networks: a role for gap-junctional coupling. J Neurophysiol 81:1274–1283.
Smolen P, Rinzel J, Sherman A (1993) Why pancreatic islets burst but single beta cells do not. The heterogeneity hypothesis. Biophys J 64:1668–1680.
Sqalli-Houssaini Y, Cazalets JR, Clarac F (1993) Oscillatory properties of the central pattern generator for locomotion in neonatal rats. J Neurophysiol 70:803–813.
Su H, Alroy G, Kirson ED, Yaari Y (2001) Extracellular calcium modulates persistent sodium current-dependent burst-firing in hippocampal pyramidal neurons. J Neurosci 21:4173–4182.
Svirskis G, Hounsgaard J (1998) Transmitter regulation of plateau properties in turtle motoneurons. J Neurophysiol 79:45–50.
Taccola G, Nistri A (2007) Differential modulation by tetraethylammonium of the processes underlying network bursting in the neonatal rat spinal cord in vitro. Neuroscience 146:1906–1917.
Tazerart S, Vinay L, Brocard F (2007a) Persistent sodium current-dependent pacemaker properties in the central pattern generator for locomotion in rodents. Soc Neurosci Abstr 33:406.3.
Tazerart S, Viemari JC, Darbon P, Vinay L, Brocard F (2007b) Contribution of persistent sodium current to locomotor pattern generation in neonatal rats. J Neurophysiol 98:613–628.
Theiss RD, Heckman CJ (2005) Systematic variation in effects of serotonin and norepinephrine on repetitive firing properties of ventral horn neurons. Neuroscience 134:803–815.
Theiss RD, Kuo JJ, Heckman CJ (2007) Persistent inward currents in rat ventral horn neurones. J Physiol 580:507–522.
Thoby-Brisson M, Ramirez JM (2001) Identification of two types of inspiratory pacemaker neurons in the isolated respiratory neural network of mice. J Neurophysiol 86:104–112.
Tresch MC, Kiehn O (2000) Motor coordination without action potentials in the mammalian spinal cord. Nat Neurosci 3:593–599.
van Drongelen W, Koch H, Elsen FP, Lee HC, Mrejeru A, Doren E, Marcuccilli CJ, Hereld M, Stevens RL, Ramirez JM (2006) Role of persistent sodium current in bursting activity of mouse neocortical networks in vitro. J Neurophysiol 96:2564–2577.
Wichterle H, Lieberam I, Porter JA, Jessell TM (2002) Directed differentiation of embryonic stem cells into motor neurons. Cell 110:385–397.
Wilson JM, Hartley R, Maxwell DJ, Todd AJ, Lieberam I, Kaltschmidt JA, Yoshida Y, Jessell TM, Brownstone RM (2005) Conditional rhythmicity of ventral spinal interneurons defined by expression of the Hb9 homeodomain protein. J Neurosci 25:5710–5719.
Wilson JM, Cowan AI, Brownstone RM (2007) Heterogeneous electrotonic coupling and synchronization of rhythmic bursting activity in mouse Hb9 interneurons. J Neurophysiol 98:2370–2381.
Wilson JM, Cowan AI, Brownstone RM (2008) Hb9 interneurons: reply to Ziskind-Conhaim and Hinckley. J Neurophysiol 99:1047–1049.
Xiong Z, Lu W, MacDonald JF (1997) Extracellular calcium sensed by a novel cation channel in hippocampal neurons. Proc Natl Acad Sci U S A 94:7012–7017.
Yue C, Yaari Y (2004) KCNQ/M channels control spike afterdepolarization and burst generation in hippocampal neurons. J Neurosci 24:4614–4624.
Yue C, Remy S, Su H, Beck H, Yaari Y (2005) Proximal persistent Na^+ channels drive spike afterdepolarizations and associated bursting in adult CA1 pyramidal cells. J Neurosci 25:9704–9720.
Zhong G, Díaz-Ríos M, Harris-Warrick RM (2006a) Serotonin modulates the properties of ascending commissural interneurons in the neonatal mouse spinal cord. J Neurophysiol 95:1545–1555.
Zhong G, Díaz-Ríos M, Harris-Warrick RM (2006b) Intrinsic and functional differences among commissural interneurons during fictive locomotion and serotonergic modulation in the neonatal mouse. J Neurosci 26:6509–6517.
Zhong G, Masino MA, Harris-Warrick RM (2007) Persistent sodium currents participate in fictive locomotion generation in neonatal mouse spinal cord. J Neurosci 27:4507–4518.
Ziskind-Conhaim L, Hinckley CA (2008) Hb9 versus type 2 interneurons. J Neurophysiol 99:1044–1046.